

## Novel Substrate-Based Inhibitors of Human Glutamate Carboxypeptidase II with Enhanced Lipophilicity<sup>†</sup>

Anna Plechanová,<sup>‡,§,●</sup> Youngjoo Byun,<sup>||,⊥,●</sup> Glenda Alquicer,<sup>#</sup> L'ubica Škultétyová,<sup>#</sup> Petra Mlčochová,<sup>‡,§</sup> Adriana Němcová,<sup>‡</sup> Hyung-Joon Kim,<sup>||</sup> Michal Navrátil,<sup>‡,§</sup> Ronnie Mease,<sup>||</sup> Jacek Lubkowski,<sup>∞</sup> Martin Pomper,<sup>||</sup> Jan Konvalinka,<sup>‡,§</sup> Lubomír Rulíšek,<sup>‡</sup> and Cyril Barinka<sup>\*,#</sup>

<sup>†</sup>Institute of Organic Chemistry and Biochemistry, Gilead Sciences Research Center at IOCB, Academy of Sciences of the Czech Republic, Flemingovo náměstí 2, 166 10 Praha 6, Czech Republic

<sup>§</sup>Department of Biochemistry, Faculty of Natural Science, Charles University in Prague, Hlavova 2030, Prague, Czech Republic

<sup>||</sup>Russell H. Morgan Department of Radiology and Radiological Sciences, Johns Hopkins Medical Institutions, 1550 Orleans Street, Baltimore, Maryland 21231, United States

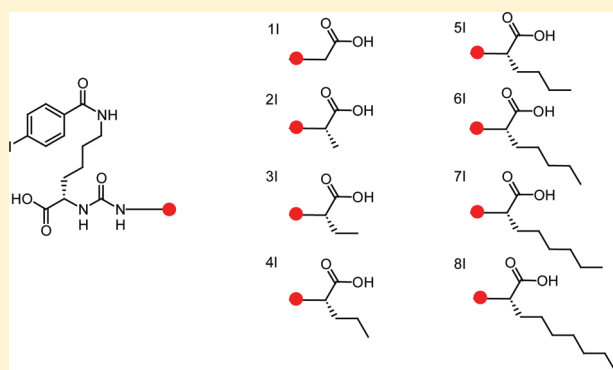
<sup>⊥</sup>College of Pharmacy, Korea University, Sejong-ro, Jochiwon-eup, Yeongi-gun, Chungnam 339-700, South Korea

<sup>#</sup>Institute of Biotechnology, Academy of Sciences of the Czech Republic, Videnska 1083, 14200 Praha 4, Czech Republic

<sup>∞</sup>Center for Cancer Research, National Cancer Institute at Frederick, Frederick, Maryland 21702, United States

### **S** Supporting Information

**ABSTRACT:** Virtually all low molecular weight inhibitors of human glutamate carboxypeptidase II (GCPII) are highly polar compounds that have limited use in settings where more lipophilic molecules are desired. Here we report the identification and characterization of GCPII inhibitors with enhanced lipophilicity that are derived from a series of newly identified dipeptidic GCPII substrates featuring nonpolar aliphatic side chains at the C-terminus. To analyze the interactions governing the substrate recognition by GCPII, we determined crystal structures of the inactive GCPII(E424A) mutant in complex with selected dipeptides and complemented the structural data with quantum mechanics/molecular mechanics calculations. Results reveal the importance of nonpolar interactions governing GCPII affinity toward novel substrates as well as formerly unnoticed plasticity of the S1' specificity pocket. On the basis of those data, we designed, synthesized, and evaluated a series of novel GCPII inhibitors with enhanced lipophilicity, with the best candidates having low nanomolar inhibition constants and clogD > -0.3. Our findings offer new insights into the design of more lipophilic inhibitors targeting GCPII.



### ■ INTRODUCTION

Human glutamate carboxypeptidase II (GCPII) is a transmembrane metallopeptidase with the expression pattern restricted primarily to nervous and prostatic tissues.<sup>1–3</sup> As the expression levels of the prostate form of the enzyme are highly elevated in prostate carcinoma and its metastases, GCPII serves as a membrane-bound marker for prostate cancer imaging and experimental therapy.<sup>4–8</sup>

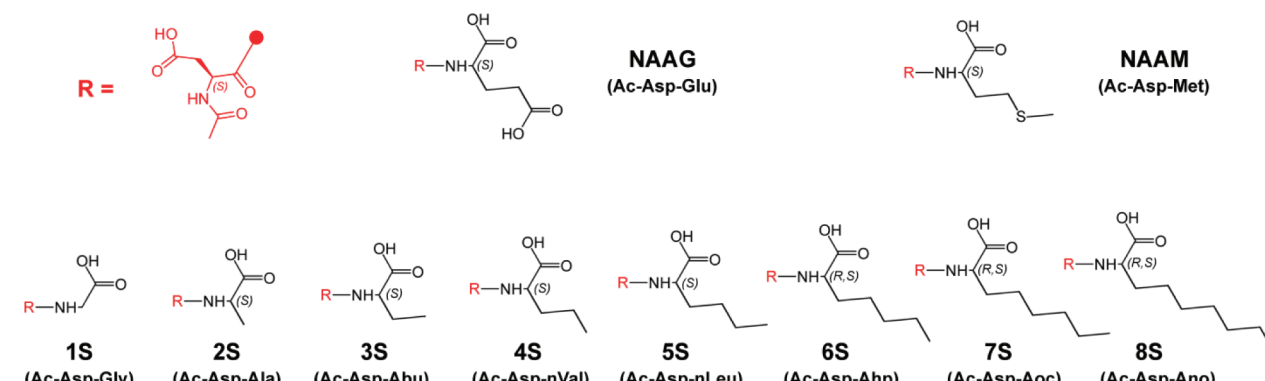
Within the nervous system, GCPII catabolizes *N*-Ac-Asp-Glu (NAAG), the dipeptidic neuropeptide, liberating glutamate into the extrasynaptic space.<sup>1</sup> Both NAAG and glutamate act as potent neurotransmitters, and their extracellular concentrations must be tightly regulated to secure normal brain functioning. Not surprisingly, dysregulated NAAG (and glutamate) metabolism and signaling are associated with a number of neurological disorders.<sup>9</sup> Given the intimate involvement of GCPII in NAAG (glutamate) metabolism, the modulation of its enzymatic activity

by small-molecule ligands is considered a viable option for the treatment and diagnosis of a variety of pathologies that involve glutamatergic transmission. Indeed, GCPII inhibitors have demonstrated efficacy in experimental models of stroke,<sup>10</sup> diabetic neuropathy,<sup>11</sup> amyotrophic lateral sclerosis,<sup>12</sup> neuropathic and inflammatory pain,<sup>13–15</sup> schizophrenia,<sup>16</sup> and drug addiction.<sup>17,18</sup> Additionally, radiolabeled GCPII-specific ligands were used to quantitatively visualize GCPII in rodent and human tissue *ex vivo*,<sup>19,20</sup> thus expanding their use into the diagnostic area.

Effective targeting of GCPII residing in nervous tissue requires inhibitors that can penetrate the neuronal compartment. That can be achieved by designing inhibitors that can leverage active transport mechanisms or by using lipophilic compounds with enhanced penetration across the blood–brain barrier. As the

Received: June 22, 2011

Published: September 19, 2011

Table 1. Formulas and Kinetic Parameters of Novel GCPII Dipeptidic Substrates<sup>a</sup>


compd	$K_M$ ( $\mu M$ )	$k_{cat}$ ( $s^{-1}$ )	$k_{cat}/K_M$ ( $L \cdot mmol^{-1} \cdot s^{-1}$ )
1S	NA <sup>b</sup>	NA <sup>b</sup>	NA <sup>b</sup>
2S	85 ± 21	0.23 ± 0.05	2.7
3S	29 ± 8	0.25 ± 0.03	8.6
4S	31 ± 12	0.42 ± 0.05	13.5
5S	19 ± 4	0.24 ± 0.01	12.6
6S	12 ± 1	0.44 ± 0.04	36.7
7S	8 ± 2	0.60 ± 0.03	75.0
8S	10 ± 2	0.62 ± 0.10	62.0
NAAM	24.8 ± 2.9 <sup>c</sup>	0.07 ± 0.002	2.9
NAAG	1.2 ± 0.5 <sup>d</sup>	1.1 ± 0.2 <sup>d</sup>	930 <sup>d</sup>

<sup>a</sup> Ac-Asp-Glu (NAAG), natural GCPII substrate in mammalian nervous system; Ac-Asp-Met (NAAM), non-natural GCPII substrate from the dipeptidic library screen; 1S...8S, novel GCPII dipeptidic substrates featuring nonpolar aliphatic side chain at the P1' position. The kinetic parameters were determined by saturation kinetics employing precolumn derivatization of the reaction products (i.e., released C-terminal amino acids) with AccQ-Fluor, followed by HPLC separation on a C18(2) Luna column and fluorimetric detection. <sup>b</sup> Not analyzed, substrate hydrolysis below the detection limit. <sup>c</sup> From ref 21. <sup>d</sup> From ref 29.

early efforts in identifying low molecular weight GCPII inhibitors relied mainly on the knowledge of GCPII substrate specificity, the two major categories of GCPII-specific inhibitors that exist at present are either analogues of NAAG (the GCPII substrate) or derivatives of glutamic acid (the reaction product). Consequently, nearly all currently used GCPII inhibitors are highly polar with their total molecular charges under physiological pH conditions ranging typically between -2 and -3 and with lower likelihood of CNS penetration. The design of GCPII-specific inhibitors with increased lipophilicity/hydrophobicity is therefore highly desirable, with the ultimate goal of improving bioavailability and tissue penetration while maintaining potency and specificity for the use in clinical practice.

In our previous work, we reported the analysis of the substrate specificity of human GCPII, and in addition to the known GCPII substrates featuring C-terminal glutamate, we identified P1' methionine as a residue effectively recognized by the enzyme.<sup>21</sup> Taking into the account the substitution of the glutamate negatively charged side chain by the more hydrophobic side chain of methionine, we hypothesized that in addition to salt bridges and/or hydrogen bonds, nonpolar interactions at the S1' site of GCPII are likely to play an important role in the positioning of the C-terminal amino acid residue of GCPII substrates. These arguments are also consistent with our other findings concerning the importance of specific amino acid residues in the GCPII S1 and S1' sites,<sup>22</sup> the detailed study of GCPII reaction mechanism,<sup>23</sup> and previously reported series of GCPII-specific inhibitors.<sup>7,24–28</sup>

The aim of this work is to explore new directions in the rational design of GCPII inhibitors by increasing their lipophilicity and to explain in detail the observed nonpolar interaction patterns. To achieve this goal, we use a combination of experimental and theoretical approaches including X-ray crystallography, site-directed mutagenesis, and hybrid quantum mechanical and molecular mechanical (QM/MM) calculations. Starting from the detailed characterization of GCPII–methionine interactions within the S1' pocket, we designed and characterized novel GCPII substrates featuring aliphatic side chains at the C-terminal amino acid. Finally, on the basis of our kinetic data, we synthesized and evaluated a series of novel substrate-based GCPII inhibitors with enhanced lipophilicity.

## RESULTS

**Novel GCPII Substrates: Ac-Asp-Ala...Ac-Asp-Ano Series.** Since dipeptides with the C-terminal methionine, but not with branched hydrophobic amino acids such as valine or leucine, are efficiently hydrolyzed by human GCPII,<sup>21,29</sup> we hypothesized that the enzyme might be able to process dipeptides bearing an unbranched, aliphatic side chain at the C-terminal moiety. To test this prediction, we analyzed the hydrolysis of a series of eight dipeptides by recombinant human GCPII (rhGCPII, Table 1). The series was chosen to examine systematically the effect of P1' aliphatic side chain length on the hydrolysis by rhGCPII. The substrate cleavage was followed by high-performance liquid

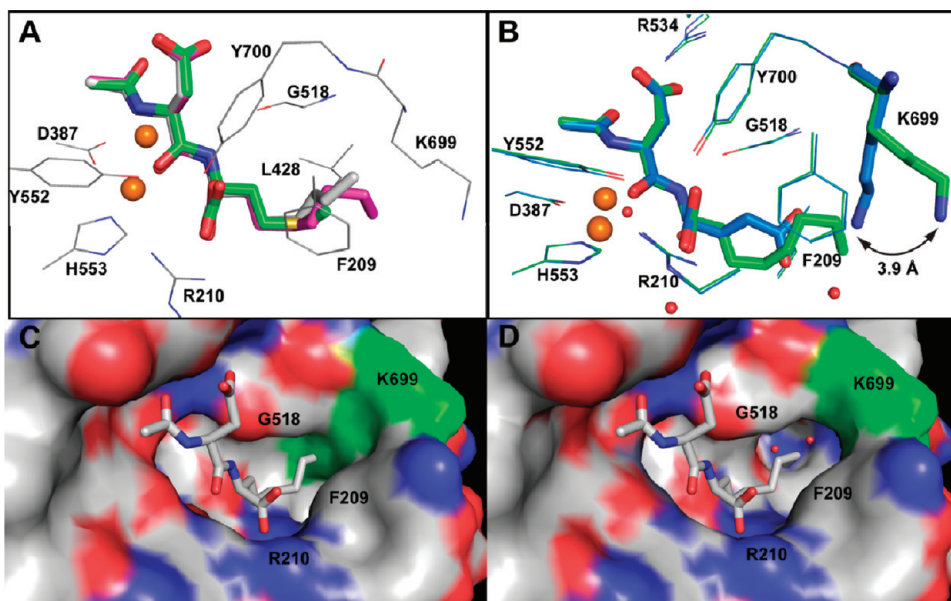


**Figure 1.** (A) Superposition of NAAM, 7S, and 8S substrates in the substrate binding pocket of GCPII(E424A). The substrates are shown in stick representation with carbon atoms colored green (NAAM), gray (7S), and magenta (8S). Selected GCPII residues surrounding the binding pocket are shown in line representation. The zinc ions are shown as orange spheres. (B) Superposition of NAAG (PDB code 3BXM) 8S substrate binding sites of GCPII. Substrates and the amino acids Lys699 are shown in stick representation, zinc ions and waters as orange and red spheres, respectively. Selected GCPII residues surrounding the binding pocket are shown in line representation. Atoms are colored as follows: cyan (NAAG carbon), green (8S carbon), blue (nitrogen), and red (oxygen). Note the displacement of the Lys699 side chain by 3.9 Å in the 8S complex (green) due to steric clash with the 8S side chain. (C, D) S1' pocket plasticity defined by the "Lys699 swing". (C) Composite figure showing GCPII substrate binding site (surface representation) derived from the NAAG (PDB code 3BXM) complex and 8S (stick representation). Note the steric clash between the side chain of Lys699 (green) and the side chain of the C-terminal residue in 8S. (D) GCPII substrate binding site (surface representation) from the complex with 8S (stick representation). The swing-out of the Lys699 side chain (green) enlarges the S1' pocket to accommodate longer (or more bulky) side chains of P1' part of substrates/inhibitors. The figure was generated using The PyMOL Molecular Graphics System, version 0.99, Schrödinger, LLC.

chromatography (HPLC), and the results are summarized in Table 1. Except for 1S (Ac-Asp-Gly), a substrate lacking a side chain at the C-terminal amino acid, all other dipeptidic substrates tested were hydrolyzed by rhGCPII. The least efficient substrate in this series was 2S (Ac-Asp-Ala), i.e., the substrate with the shortest amino acid side chain, and gradual extension of the hydrocarbon side chain of the C-terminal amino acid resulted in the monotonic improvement of the overall catalytic efficiency. This trend is documented by the fact that compared to Ac-Asp-Ala, the rhGCPII hydrolysis of 8S (Ac-Asp-Ano), the dipeptide with the longest (heptyl) C-terminal side chain, is approximately 20-fold more efficient (Table 1).

**rhGCPII(E424A)/Substrate Complexes.** To elucidate structural features that govern interactions between GCPII and nonpolar side chains of P1' residues, we determined X-ray structures of the inactive rhGCPII(E424A) mutant<sup>23</sup> in complex with three of the biochemically characterized substrates Ac-Asp-Met (NAAM), 7S (Ac-Asp-Aoc), and 8S (Ac-Asp-Ano) at a resolution of 1.66, 1.65, and 1.70 Å, respectively. (Note: Glu424 acts as a proton shuttle during substrate hydrolysis by GCPII, and as such, it is indispensable for the enzymatic activity of the enzyme. By mutating Glu424 to alanine, we constructed the inactive GCPII(E424A) mutant that cannot hydrolyze cognate substrates and thus serves as an excellent tool for elucidating/approximating enzyme–substrate interactions.) All three structures were determined using difference Fourier methods, and the refinement statistics of the final models are summarized in the Supporting Information Table S1. The overall fold of the

rhGCPII(E424A) protein in individual complexes is nearly identical to the arrangement observed for the rhGCPII(E424A) complex with NAAG, a natural GCPII substrate reported earlier (PDB code 3BXM).<sup>23</sup> The only major structural deviations in the substrate binding cavity are observed for the Lys699 side chain that comes into contact with the side chains of C-terminal amino acids of novel substrates. The superposition of the active-site-bound substrates in the S1' pocket and their comparison to the rhGCPII(E424A)/NAAG complex are depicted in Figure 1.

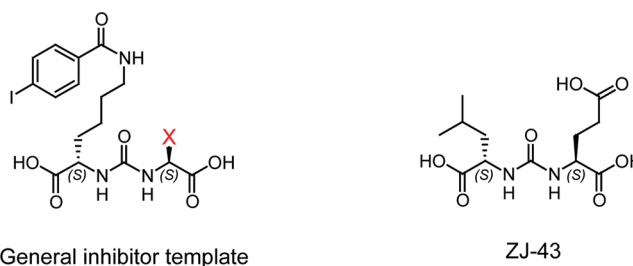
**Substrate Orientation in the GCPII Binding Pocket.** Positioning of all three dipeptides within the GCPII binding pocket can be unambiguously assigned from the electron density map and conforms to a canonical model, where the S1 pocket of GCPII is occupied by the acetyl-aspartyl moiety and the C-terminal part of a substrate extends into the S1' site. Even though an equimolar mixture of (1'-R,S)-diastereomers was used in the cases of 7S and 8S dipeptides, only the 1'-S-stereoisomers are observed in the GCPII complexes (Figure 1). That observation is consistent with known preferences of GCPII toward L-amino acids in the P1' position of substrates and (S)-stereoisomers of inhibitors.<sup>1,30</sup>

**S1' Pocket Interactions.** The enzyme–substrate interactions within the S1' site include both polar and nonpolar contacts. The arrangement of polar interactions is analogous to the polar contacts reported earlier for the rhGCPII(E424A) complex with NAAG<sup>23</sup> and includes direct hydrogen bonding/ionic interactions between the C-terminal  $\alpha$ -carboxylate and side chains of Arg210, Tyr700, and Tyr552 as well as several water mediated

Table 2. Effects of the K699S Mutation on NAAG, NAAM, and 8S Hydrolysis<sup>a</sup>

substrate	$K_M$ ( $\mu\text{M}$ )		$k_{\text{cat}}$ ( $\text{s}^{-1}$ )		$k_{\text{cat}}/K_M$ ( $\text{L}\cdot\text{mmol}^{-1}\cdot\text{s}^{-1}$ )	
	WT	K699S	WT	K699S	WT	K699S
NAAG	$1.2 \pm 0.5^b$	$40.5 \pm 22.7$	$1.1 \pm 0.2^b$	$0.34 \pm 0.08$	$930^b$	8.4
NAAM	$7.5 \pm 1.6$	$2.6 \pm 1.1$	$0.32 \pm 0.07$	$0.25 \pm 0.04$	42.7	96.2
8S	$10.4 \pm 2.5$	$2.9 \pm 0.7$	$0.62 \pm 0.10$	$0.37 \pm 0.05$	59.6	127.6

<sup>a</sup>The kinetic parameters of wild-type (WT) and mutated (K699S) GCPII toward individual substrates were determined by saturation kinetics. The reaction products were derivatized with AccQ-Fluor and separated by HPLC on a C18(2) Luna column with fluorimetric detection. <sup>b</sup>The kinetic parameters of the NAAG hydrolysis by rhGCPII were taken from ref 29 and are included here for the purpose of comparison. These values were determined by the radioenzymatic assay using <sup>3</sup>H-NAAG as a substrate.

Table 3. Inhibition of GCPII by Novel Substrate-Based Inhibitors<sup>a</sup>

inhibitor	X moiety	$K_i$ (nM)	CI (95% confidence)	MW	ClogD
ZJ-43		1.08 (0.75 <sup>b</sup> )	0.85–1.36	304.13	–6.13
1I	–H	4390 (1320 <sup>b</sup> )	3344–5762	477.04	–3.76
2I	–CH <sub>3</sub>	325	231–458	491.06	–3.41
3I	–CH <sub>2</sub> CH <sub>3</sub>	121	86–165	505.07	–2.88
4I	–(CH <sub>2</sub> ) <sub>2</sub> CH <sub>3</sub>	145 (52.3 <sup>b</sup> )	96–219	519.09	–2.35
5I	–(CH <sub>2</sub> ) <sub>3</sub> CH <sub>3</sub>	56	34–92	533.10	–1.82
6I	–(CH <sub>2</sub> ) <sub>4</sub> CH <sub>3</sub>	20	10–40	547.12	–1.29
7I	–(CH <sub>2</sub> ) <sub>5</sub> CH <sub>3</sub>	72	43–123	561.13	–0.76
8I	–(CH <sub>2</sub> ) <sub>6</sub> CH <sub>3</sub>	29	21–38	575.15	–0.23
9I	–Met	23	12–44	551.40	–2.37
10I (DCIBzL)	–Glu	0.01 <sup>b</sup>	0.007–0.013	549.06	–5.16

<sup>a</sup>Inhibitory properties of the novel compounds were determined using the Amplex Red assay, and the results are summarized in the table. <sup>b</sup>Values from ref 32.

contacts. On the other hand, two hydrogen-bonding interactions between the glutamate  $\gamma$ -carboxylate and the Asn257 and Lys699 side chains are lost in the case of dipeptides with P1' nonpolar side chains. Instead, the positioning of the C-terminal aliphatic side chain relies mainly on nonpolar contacts with the side chains of Phe209, Asn257, Leu428, Lys699 and main chains of Gly427 and Gly517.

**Flexibility of the Lys699 Side Chain Shapes the S1' Pocket.** Extended C-terminal side chains of several novel substrates (most prominently 7S and 8S) are too long ( $\sim 8.5$  Å from C $_{\alpha}$  to the terminal aminononanoic side chain carbon atom in the extended conformation) to fit conveniently into the standard-size S1' pocket observed repeatedly for glutamate-like moieties. Instead, the S1' pocket has to be reshaped to accommodate such residues. Our structural data show that the change in size and shape is realized by the out-swing of the Lys699 side chain with the positional shift of the N<sup>5</sup> by 3.9 Å. Simultaneously, the C-terminal side chains adopt a bow-shaped conformation to fill in the S1' pocket (Figure 1). Clearly, the flexibility of the Lys699 side chain is crucial for alleviating steric crowding imposed by the

presence of a bulkier substrate/inhibitor moiety, thus contributing prominently to the plasticity of the S1' pocket.

To verify the “steric crowding” hypothesis, we constructed a GCPII(K699S) mutant, where Lys699 is mutated to serine. Compared to wild-type GCPII, the K699S mutation results in approximately 3-fold stronger binding of 8S as determined by the kinetic assay (Table 2). These data suggest that the short side chain of Ser699 is more accommodating toward the bulkier C-terminal side chains of a substrate than the long Lys699 side chain. On the other hand, a much lower affinity of NAAG toward the K699S mutant ( $\sim 30$ -fold increase in the Michaelis constant compared to the wild-type enzyme) confirms the importance of the Lys699-Glu  $\gamma$ -carboxylate salt bridge for binding of compounds featuring C-terminal glutamate.

**Substrate-Based Inhibitors.** On the basis of our kinetic and structural data, we designed and evaluated a series of novel inhibitors, where the N-Ac-Asp moiety and the peptide bond of a substrate are replaced by the (4-iodobenzoylamino)hexanoyl functionality and the nonhydrolyzable urea surrogate, respectively. The rationale for the N-Ac-Asp to (4-iodobenzoylamino)hexanoyl

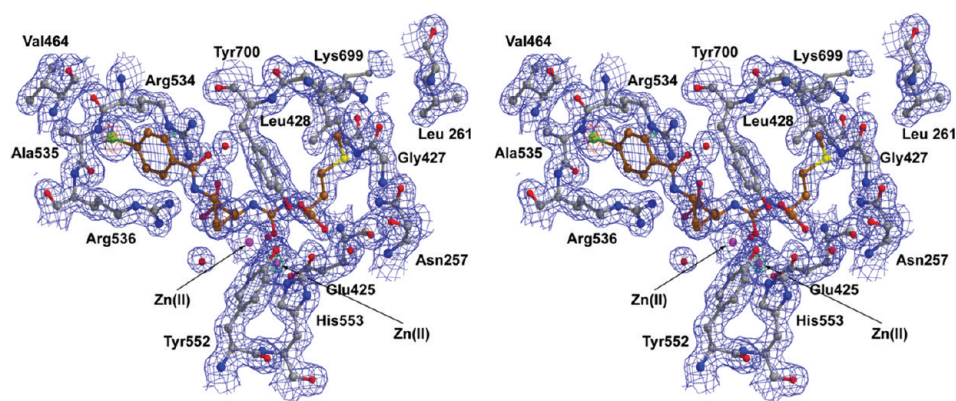


**Figure 2.** Stereoview of the electron density map of the GCPII/9I complex. The  $2F_o - F_c$  map is contoured at  $1\sigma$  (blue), and the  $F_o - F_c$  electron density maps are contoured at  $-3\sigma$  (red) and  $+3\sigma$  (green). Carbon atoms of the inhibitor and GCPII are colored brown and gray, respectively. The following coloring scheme was used for individual atoms: oxygen (red), nitrogen (blue), iodine (green), sulfur (yellow), zinc (pink).

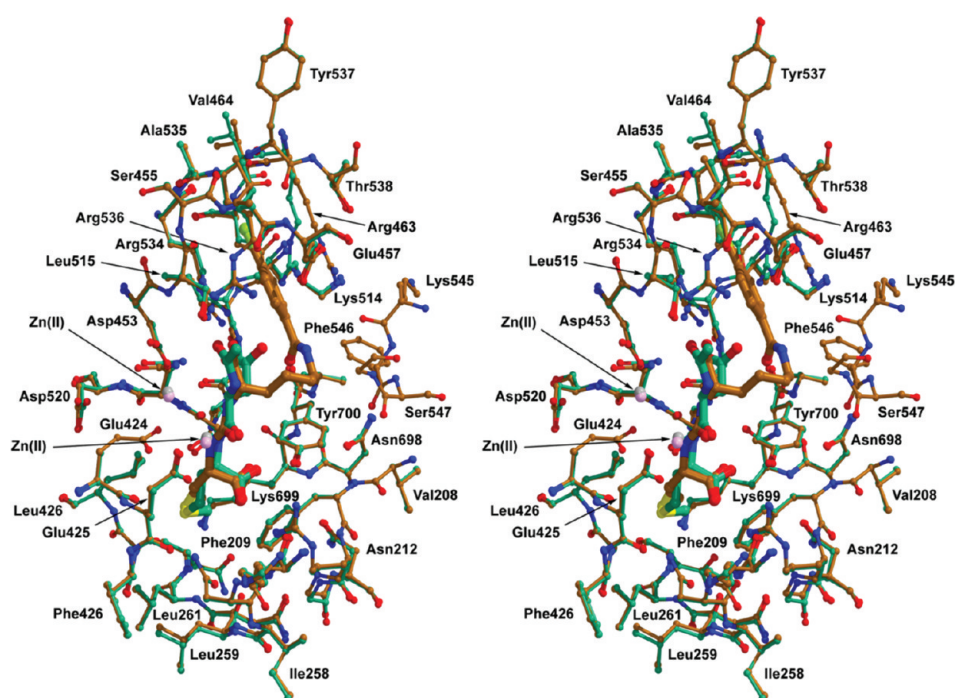


**Figure 3.** Stereoview of superimposed active site regions of GCPII/9I and GCPII(E424A)/NAAM complexes (inhibitor and its parent substrate). A fragment of the GCPII/9I (wild-type GCPII and 9I inhibitor) complex is shown in light-brown, and an equivalent fragment of the GCPII(E424A)/NAAM (the inactive mutant and NAAM substrate) complex is shown in green. The following coloring scheme was used for individual atoms: oxygen (red), nitrogen (blue), iodine (green), sulfur (yellow). Two active site zinc atoms are shown as pink spheres, and the substrate/inhibitor is shown in a thick ball-and-stick representation.

substitution was driven by our prior observation that the incorporation of this functionality into the glutamate–urea scaffold increases the affinity of resulting compounds by several orders of magnitude.<sup>24</sup> Inhibitory properties of the novel compounds were determined using the Amplex Red assay, and the results are summarized in Table 3. The  $K_i$  values in the series follow the general trend observed for the parent substrates, with the inhibitor potency increasing with the elongation of the P1' side chain. In this series, compound **II** has the lowest affinity toward GCPII ( $K_i = 4390$  nM), while the inhibition constants monotonically decrease from **II** through **6I** and plateau for compounds **6I**–**8I**, reaching low nanomolar affinity ( $\sim 20$  nM).

The “plateau effect” observed for the inhibitor series mirrors results from the kinetic measurements, pointing toward identical/similar positioning of P1' moieties of substrates/inhibitors. As a result, structural/biochemical observations for one type of ligand, substrate or inhibitor, can likely be extrapolated to the corresponding counterpart and exploited for the design of substrate-based inhibitors in general.

**GCPII/9I Complex: X-ray Structure.** To confirm the assumption that binding modes to an inhibitor and its parent substrate by GCPII are similar, we determined an X-ray structure of GCPII in complex with 9I, a urea-based inhibitor derived from NAAM, at 1.65 Å resolution. The binding mode of 9I in the GCPII

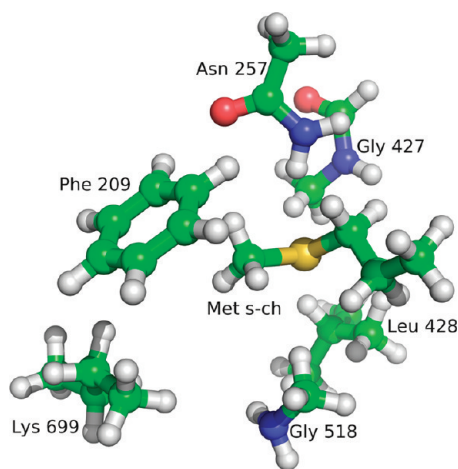


**Figure 4.** Model system used for the calculations of interaction energies, the S1' residues (side chains of Phe209, Asn257, Leu428, backbone of Gly427 and Gly518, and nonpolar part of the Lys699 side chain) interacting with the nonpolar side chains of the substrates/inhibitors. The model system truncated from the GCPII(E424A)/NAAM complex (Met side chain and model functional groups representing the key interacting residues from the enzyme) is used in the figure.

specificity pockets is unambiguously defined by the  $F_o - F_c$  omit map (Figure 2) and mirrors the orientation and positioning of **10I** (DCIBzL, a urea-based compound featuring C-terminal glutamate). More importantly, though, the C-terminal methionine in the GCPII/**9I** complex (together with surrounding GCPII side chains) spatially overlaps with the corresponding part of NAAM, its parent substrate (Figure 3). Taken together, these data suggest transferability of kinetic/enzymatic data into the inhibitory profiles of daughter compounds.

**GCPII/Ligand Complexes: QM/MM Modeling.** On the basis of the above-described crystallographic data, we carried out the QM/MM calculations to extend the experimental structural information over additional aspects of the ligand–GCPII binding such as the protonation equilibria between protein and ligand or energies associated with the enzyme ··· ligand interaction. In total, seven structures were modeled and examined, including complexes of NAAM, **7S**, and **8S** with both wild-type GCPII and the GCPII(E424A) mutant, as well as the complex of **8I** and **10I** with wild-type GCPII. Moreover, we have considered the protonation of the Glu424 residue (that acts as a proton shuttle in the GCPII catalytic cycle), which resulted in a total of 13 systems that were studied. A fairly large quantum region (~350 atoms) and a neighboring part of the protein optimized at the MM level (additional 110 amino acid residues) should allow for a sufficient degree of flexibility in the binding site.

The resulting optimized structures can be found in the Supporting Information (including partial charges on all atoms). The excellent structural agreement between the equilibrium QM/MM structures and their crystallographic counterparts allowed more detailed energy analysis of the interactions between substrates/inhibitors and GCPII (vide infra). Moreover, the QM/MM calculations yielded the equilibrium structures of the wild-type GCPII with NAAM, **7S**, **8S** and the model structure of the GCPII complex with **8I** (i.e., structures that have not been determined experimentally), which add to the already extensive structural information obtained in this study. The alignments of the calculated and experimental structures are depicted in

**Table 4.** Calculated Interaction Energies of the Model Ligands Representing S1' Residues with the P1' Side Chains of the Selected Substrates/Inhibitors Using B-LYP(+D)/TZVPP Method and QM/MM Optimized Geometries of GCPII/Ligand Complexes<sup>a</sup>

	Met	AOC	ANO
Phe209	−1.4	−2.4	−2.2
Asn257	−4.8	−1.7	−2.4
Gly427(bb)	−1.3	−1.9	−2.1
Leu428	−1.3	−2	−2.1
Gly518(bb)	−2.1	−2	−1.4
Lys699(n-p)	−0.3	−1.4	−1.6
$\Sigma E_{ij}$	−11.2	−11.4	−11.5

<sup>a</sup> All values are in kcal·mol<sup>−1</sup>.

Figure S1a–c (Supporting Information), whereas the newly predicted structures are depicted in Figure S2.

The most notable structural features of the QM/MM optimized structures not attainable from the X-ray crystallography can be summarized as follows:

(1) In wild-type complexes, a hydroxide anion, not a water molecule, bridges the two zinc ions in the active site, since the water molecule spontaneously deprotonates upon binding to the (Zn)<sub>2</sub> site. Most likely, the proton resides on the Glu424 moiety and is ready for the second step of the peptide bond cleavage as shown in the previous study.<sup>23</sup>

(2) In the complexes with the nonpolar side chains at the C-terminus, the charge of the Lys699 residue which is otherwise the key residue for the interaction with (and the recognition of) the C-terminal (P1') glutamate in GCPII natural substrates is attenuated by a chain of three water molecules that are strongly polarized by the interaction with the charged NH<sup>3+</sup> group with the O–H bonds elongated by 0.1–0.2 Å in comparison with their standard values.

(3) In QM/MM optimized structures, we have not observed any pronounced structural changes related to the protonation of the Glu424 residue, as the extra “catalytic” proton<sup>23</sup> is not directly involved in any hydrogen bond. Neither have we noticed any significant effect of the E424A mutation on the overall constitution of the GCPII active site and positioning of the substrate. The superpositions of the wild-type GCPII, GCPII(E424A), and protonated wild-type GCPII structures are given in the Supporting Information (Figures S3–S5).

**Interaction Energies of Nonpolar Side Chains with the S1' Site Residues.** We utilized the results of the QM/MM calculations to provide semiquantitative arguments to the discussions concerning the origin of the nonpolar interactions between ligands and the S1' site of GCPII. We have calculated interaction energies of the model ligands representing the side chains of Met, 2-aminooctanoic (AOC), and 2-aminononanoic (ANO) acids with the small models of interacting residues. The system is depicted in Figure 4, and the results are summarized in Table 4. It is emphasized that the results are only semiquantitative because of the simplicity of the model functional groups representing the residues, but a few observations can be made.

Concerning the overall value of the interaction energy, one may observe that for AOC and ANO side chains it is marginally higher (0.2–0.4 kcal·mol<sup>−1</sup>) than for the Met side chain. It qualitatively correlates with the observed decrease in  $K_M$  values (NAAM vs **7S** and **8S**). However, these differences are very

small, and admittedly, the same correlation does not extend to the 7S vs 8S comparison.

In the case of methionine, more than 40% of the overall interaction energy ( $-11.1 \text{ kcal}\cdot\text{mol}^{-1}$ ) with the neighboring residues comes from the interaction with Asn257 side chain ( $-4.8 \text{ kcal}\cdot\text{mol}^{-1}$ ). Other nonpolar residues contribute by  $\sim -1.5 \text{ kcal}\cdot\text{mol}^{-1}$  per residue with the exception of the nonpolar part of the Lys699 side chain (modeled as  $\text{CH}_3(\text{CH}_2)_2\text{CH}_3$ ) that contributes negligibly. For the C-terminal AOC and ANO, there is a notable increase in the interaction of Phe209 and the nonpolar part of Lys699 (by  $\sim 1 \text{ kcal/mol}^{-1}$ ) and a slight increase in the interaction energies of other nonpolar residues that more than compensates the energetic loss in the interaction of AOC/ANO with the Asn257. The same stabilizing role can be also postulated for several of our inhibitors previously published and highlights the importance of nonpolar and  $\pi$ - $\pi$  stacking interactions in biological systems.

Finally, we observed that the interaction energies between the P1' side chain of the substrate/inhibitor and the S1' residues are almost perfectly pairwise additive; i.e., the total interaction energy almost equals the sum of pair interaction energies. In summary, these calculations provide semiquantitative insight into the arguments about the origin of the hydrophobicity of the S1' site, given in this study.

## DISCUSSION

Glutamate-based functionalities are instrumental for selective targeting of human GCPII in applications ranging from prostate cancer (PCa) imaging to the experimental treatment of neurodegenerative conditions.<sup>8</sup> Since the GCPII pharmacophore (S1') pocket is "optimized" for glutamate-like scaffolds, the presence of these functionalities ensures both high affinity and specificity of corresponding inhibitors.<sup>31,32</sup> Several groups reported structure-activity relationship (SAR) studies focusing on substituting the P1' glutamate in GCPII inhibitors. Majer et al.<sup>33</sup> designed and tested a series of thiol-based inhibitors containing a benzyl moiety at the P1' position to increase lipophilicity of 2-(3-mercaptopropyl)pentanedioic acid (2-MPPA), the first orally available GCPII inhibitor. In addition to higher lipophilicity, the best candidates were found to be more potent than the parent molecule and showed effectiveness in a rat chronic constriction injury model of neuropathic pain. The Kozikowski group<sup>34</sup> applied the SAR approach using *N*-[[[(1S)-1-carboxy-3-methylbutyl]amino]carbonyl]-L-glutamic acid (ZJ-43, a urea-based NAAG analogue as a lead compound) to decrease polarity for more efficient targeting of GCPII in the nervous system, especially in the PNS. We evaluated a series of DCIBzL-based isosteres and identified several non-glutamate inhibitors with  $K_i$  values below 20 nM that exhibited selective binding to GCPII-expressing tumors by single photon emission computed tomography (SPECT-CT) imaging in mice.<sup>32</sup>

This report uses the rational design to extend and complement the above-mentioned SAR studies with the objective of preparing potent GCPII inhibitors with enhanced lipophilicity. On the basis of our earlier kinetic data, we first designed and characterized a set of novel dipeptidic GCPII substrates and provided the structural evidence for recognition of such dipeptides by GCPII. Next, we designed a series of inhibitors, where the P1' moiety is derived from the dipeptidic substrates and the P1 part features 4-iodobenzoyl- $\epsilon$ -lysine, the functionality shown by us previously to augment interactions with GCPII;<sup>24</sup> the P1 and P1' parts are

connected via a urea linker (Table 3). The most potent molecule (compound 8I) has  $K_i = 29 \text{ nM}$  and  $\text{ClogD} = -0.23$ . Although the binding affinity of 8I is markedly lower compared to the parent glutamate-based compound (29 nM vs 10 pM, respectively), its affinity is sufficient for imaging PCa.<sup>32</sup> Furthermore, substantially increased lipophilicity ( $-0.23$  vs  $-5.16$ ) can be translated into a better pharmacokinetic profile in the periphery, with increased likelihood of the penetration into the CNS. Last but not least, in the phase I human clinical trial using *N*-[*N*-[(*S*)-1,3-dicarboxypropyl]carbamoyl]-4-[<sup>18</sup>F]fluorobenzyl-L-cysteine ([<sup>18</sup>F]DCFBC),<sup>35</sup> one of the glutamate-based PET agents targeting GCPII that was developed for prostate cancer imaging, we observed somewhat increased signal from the blood pool in human subjects, suggesting potential binding of the compound to an unidentified plasma protein. The prime suspect in the case is plasma glutamate carboxypeptidase, a circulating plasma protein with 27% overall sequence identity and overlapping substrate specificity to GCPII.<sup>36,37</sup> Given the substitution of glutamate by non-natural amino acids in novel inhibitors presented here, the likelihood of off-target interactions with endogenous proteins might be less pronounced in the latter. To prove these assumptions, however, additional *in vivo* studies are needed.

For both substrate and inhibitor synthesis, 2-amino acids with pentyl to heptyl side chains were used as a racemic mixture for both substrate and inhibitor synthesis. The corresponding products (substrates and inhibitors) are therefore equimolar mixtures of two diastereomers. In the case of inhibitors, the individual diastereomers were separated by HPLC and their inhibition potency was assayed. As expected, only compounds with the (*S*)-stereochemistry at the C-terminus were inhibitory, while their (*R*)-counterparts turned out to be inactive (data not shown). In the case of substrates, a mixture of diastereomers was used for kinetic studies. Following the substrate incubation with rhGCPII for 24 h at 37 °C, we analyzed the reaction mixture using HPLC with UV detection after precolumn derivatization of released C-terminal amino acids with Marfey's reagent (1-fluoro-2,4-dinitrophenyl-5-L-alanineamide), a chiral reagent used for distinguishing (*S*)- and (*R*)-amino acids. In all cases, we observed peaks corresponding to only a single, presumably (*S*), enantiomer (data not shown). Since previously reported data suggested that GCPII is inactive toward (*R*)-amino acids at the P1' position, we concluded that only (*S*)-amino acid containing dipeptides serve as efficient substrates of rhGCPII.

The SAR studies suggest that the nonprime GCPII specificity pocket(s) are rather insensitive to structural changes of GCPII inhibitors and can accommodate (or at least tolerate) surprising diversity of functional groups of inhibitors.<sup>4,7,24,26,28,34</sup> On the contrary, the S1' (or pharmacophore) pocket in GCPII is highly selective for glutamate and glutamate-like moieties. The selectivity is achieved via an intricate network of mostly polar interactions between GCPII and an inhibitor, with the most prominent being the Arg210- $\alpha$ -carboxylate and Lys699- $\gamma$ -carboxylate ion pairing.<sup>22,31</sup> Structural data that characterize the S1' pocket as fairly compact, small-sized, and unyielding, in contrast to the much larger and quite flexible nonprime site (the funnel emanating from the active site zinc to the surface of the protein), are in agreement with these observations.

This report expands the above concept in two ways: (i) it documents for the first time substantial plasticity of the GCPII pharmacophore pocket achieved by the relocation of the Lys699 side chain leading to the considerable enlargement (by 3.9 Å) of

the S1' site. Furthermore, this work directly to S1' site; (ii) it directly demonstrates the importance of nonpolar interactions, mediated by the side chains of Phe209, Asn257, Leu428, and Lys699 for GCPII affinity toward small-molecule compounds featuring hydrophobic moieties in the P1' position. Although ionic interactions between the Arg210 guanidinium group and the  $\alpha$ -carboxylate group of the C-terminal (P1' position) residue are common to all dipeptidic substrates tested in this study, these are obviously not sufficient with respect to efficient substrate positioning and subsequent hydrolysis, as the dipeptide with glycine in the P1' position is not cleaved. Additionally, the dipeptide with a C-terminal alanine, the amino acid with the shortest side chain, in the P1' position is the least efficient GCPII substrate (see Table 1).

In summary, the new findings presented here expand the chemical space that can be explored during the rational design of GCPII inhibitors with increased lipophilicity. By linking a lipophilic "non-glutamate" C-terminal moiety to a nonpolar P1 functionality, one can design inhibitors with increased lipophilicity that are more likely to penetrate the blood–brain barrier. However, lipophilicity is only one of physicochemical parameters related to the druglike molecular properties (others being molecular weight, polar surface area, number of hydrogen bond donors/acceptors, number of rotatable bonds). In this regard, compounds presented here can be viewed as a precedent for the development of GCPII-specific inhibitor analogues, with the ultimate goal of designing the truly BBB-permeable compounds.

## CONCLUSIONS

In this study we (i) report the design and characterization of a novel set of dipeptidic GCPII substrates, (ii) provide structural and computational evidence for recognition of such dipeptidic substrates by GCPII, and (iii) report the design and evaluation of novel substrate-based GCPII inhibitors with nanomolar affinity and increased lipophilicity. Besides contributing to the understanding of GCPII function, these data also serve as a starting point for the design of "non-glutamate" small molecule GCPII ligands with the increased lipophilicity that may represent a novel and important class of inhibitors of GCPII.

## EXPERIMENTAL SECTION

**Wild-Type rhGCPII Expression and Purification.** The cloning, expression, and purification of recombinant human GCPII (rhGCPII) have been described previously.<sup>21</sup> Briefly, the extracellular part of human glutamate carboxypeptidase II, which spans amino acid residues 44–750, was cloned into the pMT/BiP/V5-His A plasmid (Invitrogen, Carlsbad, U.S.), and the recombinant protein (designated rhGCPII) was expressed in *Drosophila* Schneider's S2 cells and purified to homogeneity.

**Expression and Purification of rhGCPII(E424A) and rhGCPII(K699S) Mutants.** Cloning, expression, and purification of the rhGCPII(E424A) and rhGCPII(K699S) mutants have been described elsewhere.<sup>22,23</sup> In short, desired mutations were introduced into a GCPII coding sequence using QuikChange site-directed mutagenesis kit (Stratagene, La Jolla, CA, U.S.) and the mutated protein expressed in S2 cells. Purification protocols included ion-exchange chromatography steps (QAE-Sephadex A50, source S15) followed by affinity chromatography on lentil lectin and size-exclusion chromatography on a Superdex 200 column. The final protein preparations were >95% pure as determined by silver-stained SDS–PAGE (data not shown). For crystallization experiments, purified rhGCPII(E424A) was dialyzed against 20 mM MOPS, 20 mM NaCl, pH 7.4, and concentrated to 8.7 mg/mL.

**Crystallization and Data Collection.** The rhGCPII(E424A) stock solution was mixed with  $1/10$  volume of 100 mM aqueous solutions of NAAM, 7S, and 8S. For the GCPII/9I complex, rhGCPII stock solution (8 mg/mL) was mixed with  $1/10$  volume of 9I (3 mM final concentration). The protein/dipeptide or protein/inhibitor mixtures were combined with an equal volume of the reservoir solution containing 33% (v/v) pentaerythritol propoxylate PO/OH 5/4 (Hampton Research), 0.5% (w/v) PEG 3350, and 100 mM Tris-HCl, pH 8.0. Crystals were grown from 2  $\mu$ L droplets by the hanging-drop vapor-diffusion method at 293 K. For each complex, the diffraction intensities were collected from a single crystal at 100 K using synchrotron radiation ( $\lambda = 1.00 \text{ \AA}$ ) at the SER-CAT beamline 22-ID at the Advanced Photon Source (Argonne, IL, U.S.) equipped with a MAR225 CCD detector. The data sets were indexed, integrated, and scaled using the HKL software package (Table S1).<sup>38</sup>

**Structure Determination and Refinement.** Structure determination of GCPII complexes presented here were carried out using difference Fourier methods with the ligand-free rhGCPII (PDB code 2OOT)<sup>39</sup> as a starting model. Calculations were performed with the program Refmac 5.5,<sup>40</sup> and the refinement protocol was interspersed with manual corrections to the model employing the program Coot.<sup>41</sup> The restraints library and the coordinate files for individual inhibitors were prepared using the PRODRG server,<sup>42</sup> and the inhibitors/substrates were fitted into the positive electron density map in the final stages of the refinement. Approximately 1% of the randomly selected reflections were kept aside for cross-validation ( $R_{\text{free}}$ ) during the refinement process. The quality of the final models was evaluated using MolProbity.<sup>43</sup> The data collection and refinement statistics are summarized in Table S1. Atomic coordinates of the present structures together with the experimental structure factor amplitudes were deposited at the RCSB Protein Data Bank under accession numbers 3SJX [GCPII-(E424A)/NAAM], 3SJG [GCPII(E424A)/7S], 3SJE [GCPII(E424A)/8S], and 3SJF [GCPII/9I].

**Substrate Synthesis.** Glycine, (S)-alanine, (S)-norleucine, (S)-methionine, (S)-aminobutyric acid, (S)-glutamic acid, and (S)-norvaline were purchased from Sigma. (S,R)-forms of 2-aminoheptanoic, octanoic, and nonanoic acids were purchased from Fluka. N-Acetylated dipeptides were synthesized using standard Fmoc-based approach on a Wang hydroxymethylphenyl-functionalized resin.<sup>44</sup> The identity and purity of the peptides were checked by mass spectrometry, reversed-phase HPLC, and amino acid analysis, and the purity was determined to be >95% (data not shown).

**Determination of Kinetic Constants.** Kinetic constants of N-terminally acetylated dipeptidic substrates were determined by high-performance liquid chromatography with fluorimetric detection (excitation 250 nm, emission 395 nm) of precolumn derivatized amino acids. Typically, 1–2  $\mu$ g/mL rhGCPII in 20 mM MOPS, 20 mM NaCl, pH 7.4, was reacted with 5–300  $\mu$ M relevant substrate for 30 min at 37 °C in a final volume of 120  $\mu$ L. The reaction was stopped by the addition of 20  $\mu$ L of 100 mM EDTA, pH 9.2, and the pH of the reaction mixture was adjusted by the addition of 40  $\mu$ L of 100 mM borate buffer, pH 9.0. The released amino acids were derivatized using 20  $\mu$ L of 2.5 mM AccQ-Fluor reagent (Waters, Milford, MA, U.S.) dissolved in acetonitrile. Then 30  $\mu$ L of the resulting mixture was applied to a Luna C18(2) column (250 mm  $\times$  4.6 mm, 5  $\mu$ m particle size, Phenomenex) mounted to a Waters Alliance 2795 system equipped with a Waters 2475 fluorescence detector.

**Synthesis of GCPII Inhibitors.** Some of the tested inhibitors (1I, 4I, DCIBzL, and 9I) were already reported previously by our laboratory.<sup>32</sup> The other GCPII inhibitors (2I, 3I, 5I–8I) were prepared by a general procedure as follows.

To N<sup>t</sup>-Boc-L-lysine *tert*-butyl ester hydrochloric acid (339 mg, 1 mmol) in 20 mL of CH<sub>2</sub>Cl<sub>2</sub> at –78 °C was added triphosgene (98 mg, 0.33 mmol) followed by triethylamine (1 mL). The reaction mixture was



stirred at  $-78\text{ }^{\circ}\text{C}$  for 1 h, and the dry ice/acetone bath was removed. The stirring was continued for another 30 min at room temperature and the reaction mixture cooled back to  $-78\text{ }^{\circ}\text{C}$ . To the reaction mixture were added the individual amino acid (1 mmol) in anhydrous DMF (10 mL) and triethylamine (1 mL). After the mixture was stirred overnight, the excess solvent was removed under reduced pressure and the residue was purified by reverse phase HPLC to give urea compounds (20–50% yield). The urea compounds (0.1 mmol) were dissolved in 1 mL of TFA and stirred at room temperature for 60 min. The completion of the deprotection reaction was monitored by ESI-MS. Excess TFA was removed by reduced pressure. The residue was dissolved in DMF (5 mL) and triethylamine (0.5 mL), followed by the addition of 4-iodosuccinimide benzoate (0.12 mmol). The reaction mixture was stirred at room temperature for 3 h. The excess solvent was removed and the residue was purified by reverse phase HPLC to give the target compounds (40–60% yield). The final purity of inhibitors was >95% as determined by analytical HPLC.

**(S)-2-(3-((S)-1-Carboxyethyl)ureido)-6-(4-iodobenzamido)hexanoic Acid (2I).** HPLC conditions:  $\text{H}_2\text{O}/\text{CH}_3\text{CN}$  (0 min, 90/10  $\rightarrow$  30 min, 50/50, 0.1% TFA), flow rate 3 mL/min, retention time 23 min.  $^1\text{H}$  NMR (400 MHz,  $\text{H}_2\text{O}-d_2$ )  $\delta$ : 8.17 (d,  $J = 8.0$  Hz, 2H), 7.80 (d,  $J = 7.2$  Hz, 2H), 4.40–4.44 (m, 2H), 3.41–3.44 (m, 2H), 1.95–2.05 (m, 2H), 1.86–1.89 (m, 2H), 1.67–1.72 (m, 2H).  $[\text{M} + \text{H}]$  calculated for  $\text{C}_{17}\text{H}_{22}\text{IN}_3\text{O}_6$  492.1, found 491.9. Yield: 21%.

**(S)-2-(3-((S)-1-Carboxypropyl)ureido)-6-(4-iodobenzamido)hexanoic Acid (3I).** HPLC conditions:  $\text{H}_2\text{O}/\text{CH}_3\text{CN}$  (0 min, 75/25  $\rightarrow$  30 min, 40/60, 0.1% TFA), flow rate 3 mL/min, retention time 13 min.  $^1\text{H}$  NMR (400 MHz,  $\text{CD}_3\text{CN}$ )  $\delta$ : 7.81 (d,  $J = 6.8$  Hz, 2H), 7.46 (d,  $J = 6.8$  Hz, 2H) 4.08 (m, 1H), 4.01 (m, 1H), 3.26 (d,  $J = 6.8$  Hz, 2H), 1.70–1.75 (m, 2H), 1.63–1.68 (m, 2H), 1.60–1.64 (m, 2H), 1.32–1.38 (m, 2H), 0.84 (t,  $J = 7.2$  Hz, 3H).  $[\text{M} + \text{H}]$  calculated for  $\text{C}_{18}\text{H}_{24}\text{IN}_3\text{O}_6$  506.1, found 505.8. Yield: 19%.

**(S)-2-(3-((S)-1-Carboxypentyl)ureido)-6-(4-iodobenzamido)hexanoic Acid (5I).** HPLC conditions:  $\text{H}_2\text{O}/\text{CH}_3\text{CN}$  (0 min, 75/25  $\rightarrow$  30 min, 40/60, 0.1% TFA), flow rate 3 mL/min, retention time 15 min.  $^1\text{H}$  NMR (400 MHz,  $\text{MeOH}-d_4$ )  $\delta$ : 7.82 (d,  $J = 7.2$  Hz, 2H), 7.56 (d,  $J = 7.2$  Hz, 2H), 4.25 (m, 1H), 4.22 (m, 1H), 3.31–3.39 (m, 2H), 1.83–1.89 (m, 2H), 1.62–1.67 (m, 4H), 1.45–1.49 (m, 2H), 1.32–1.39 (m, 4H), 0.89 (t, 3H).  $[\text{M} + \text{H}]$  calculated for  $\text{C}_{20}\text{H}_{28}\text{IN}_3\text{O}_6$  534.1, found 533.8. Yield: 17%.

**(S)-2-(3-((S)-1-Carboxyhexyl)ureido)-6-(4-iodobenzamido)hexanoic Acid (6I).** HPLC conditions:  $\text{H}_2\text{O}/\text{CH}_3\text{CN}$  (58/42, 0.1% TFA), flow rate 3 mL/min, retention time 13.5 min.  $^1\text{H}$  NMR (400 MHz,  $\text{CD}_3\text{CN}$ )  $\delta$ : 7.80 (d,  $J = 7.2$  Hz, 2H), 7.49 (d,  $J = 7.2$  Hz, 2H), 4.13–4.18 (m, 1H), 4.08–4.12 (m, 1H), 3.27 (t,  $J = 6.8$  Hz, 2H), 1.86–1.89 (m, 1H), 1.74–1.78 (m, 2H), 1.62–1.66 (m, 3H), 1.52–1.55 (m, 2H), 1.29–1.37 (m, 6H), 0.87 (t,  $J = 6.2$  Hz, 3H).  $[\text{M} + \text{H}]$  calculated for  $\text{C}_{21}\text{H}_{30}\text{IN}_3\text{O}_6$  548.2, found 547.8. Yield: 18%.

**(S)-2-(3-((S)-1-Carboxyheptyl)ureido)-6-(4-iodobenzamido)hexanoic Acid (7I).** HPLC conditions:  $\text{H}_2\text{O}/\text{CH}_3\text{CN}$  (58/42, 0.1% TFA), flow rate 3 mL/min, retention time 16.5 min.  $^1\text{H}$  NMR (400 MHz,  $\text{CD}_3\text{CN}$ )  $\delta$ : 7.82 (d,  $J = 7.2$  Hz, 2H), 7.50 (d,  $J = 7.2$  Hz, 2H), 4.15–4.18 (m, 1H), 4.09–4.12 (m, 1H), 3.30 (t,  $J = 6.8$  Hz, 2H), 1.83–1.89 (m, 1H), 1.62–1.67 (m, 3H), 1.45–1.49 (m, 2H), 1.26–1.38 (m, 10H), 0.89 (t,  $J = 6.2$  Hz, 3H).  $[\text{M} + \text{H}]$  calculated for  $\text{C}_{22}\text{H}_{32}\text{IN}_3\text{O}_6$  562.1, found 561.9. Yield: 16%.

**(S)-2-(3-((S)-1-Carboxyoctyl)ureido)-6-(4-iodobenzamido)hexanoic Acid (8I).** HPLC conditions:  $\text{H}_2\text{O}/\text{CH}_3\text{CN}$  (58/42, 0.1% TFA), flow rate 3 mL/min, retention time 19.5 min.  $^1\text{H}$  NMR (400 MHz,  $\text{CD}_3\text{CN}$ )  $\delta$ : 7.79 (d,  $J = 8.0$  Hz, 2H), 7.48 (d,  $J = 8.0$  Hz, 2H), 4.11–4.16 (m, 1H), 4.04–4.08 (m, 1H), 3.26 (t,  $J = 6.8$  Hz, 2H), 1.73–1.81 (m, 1H), 1.52–1.63 (m, 3H), 1.32–1.38 (m, 2H), 1.17–1.30 (m, 12H), 0.88 (t,  $J = 6.2$  Hz, 3H).  $[\text{M} + \text{H}]$  calculated for  $\text{C}_{23}\text{H}_{34}\text{IN}_3\text{O}_6$  576.1, found 575.8. Yield: 14%.

**In Vitro GCPII Inhibitory Constants.** Inhibition constants were determined using a fluorescence-based assay according to a previously reported procedure.<sup>45</sup> Briefly, lysates of LNCaP cell extracts (25  $\mu\text{L}$ ) were incubated with the inhibitor (12.5  $\mu\text{L}$ ) in the presence of 4  $\mu\text{M}$  NAAG (12.5  $\mu\text{L}$ ) for 120 min. The amount of the released glutamate was determined by incubating with a working solution (50  $\mu\text{L}$ ) of the Amplex Red glutamic acid kit (Invitrogen Corp., CA, U.S.) for 60 min. The fluorescence was measured using a VICTOR<sup>3V</sup> multilabel plate reader (Perkin-Elmer Inc., Waltham, MA, U.S.) with excitation at 490 nm and emission at 640 nm. Inhibition curves were determined using semilog plots, and  $\text{IC}_{50}$  values were calculated. Assays were performed in triplicate. Enzyme inhibitory constants ( $K_i$ ) were generated using the Cheng–Prusoff conversion. Data analysis was performed using GraphPad Prism, version 4.00, for Windows (GraphPad Software, San Diego, CA).

**Quantum Chemical Calculations and QM/MM Modeling.** All QM/MM calculations were carried out with the COMQUM program.<sup>46</sup> In the current version, the program uses Turbomole 5.7<sup>47</sup> for the QM part and AMBER 8 (University of California, San Francisco, U.S.) with the Cornell force field<sup>48</sup> for the MM part. The details of the QM/MM procedure that are essentially identical to the ones described in ref 23 can be found in the Supporting Information.

**Protein (GCPII) Setup.** All structural models used in QM/MM calculations were based on the reported crystal structures and on our previous work<sup>23</sup> where we carefully described the strategy to include missing loops, addition of hydrogens, protonation states of His residues, and construction of solvation sphere, including initial simulated annealing protocol leading to the optimization of positions of all the atoms missing in the crystal structures. All these structural details can be found in the PDB files deposited. Therefore, starting from the QM/MM optimized structure of the NAAG (GCPII substrate) complexed with the enzyme,<sup>23</sup> we have replaced NAAG with the studied substrates/inhibitors (NAAM, 7S, 8S, 8S, 8I, 10I) using their experimental crystal structures as templates. In case of 8I, for which the crystal structure has not been yet determined, we used GCPII/DCIBZL and GCPII-(E424A)/7S structures as templates for positioning their P1 and P1' parts, respectively. Because of the high similarity of the structures, we considered this approach as physically more sound, since the (highly optimized) QM/MM structure already contained all hydrogen atoms and missing parts of the protein. This approach is also justified a posteriori by an excellent agreement of the equilibrium QM/MM and crystal structures for a given enzyme/inhibitor complex. The only significant structural change involved the Lys699 residue which swings by  $\sim 3.5$  Å upon binding of the inhibitors with longer alkyl chains as described above. Also, we have tried to carefully adapt the positions of two to three water molecules in the vicinity of the active site to match their positions in the crystal structures. The quantum region in the calculations consisted of the following residues: two  $\text{Zn}^{2+}$  ions, bringing hydroxide moiety, inhibitor, side chains of Phe209, Arg210, Asn257, His377, Asp387, Glu424, Glu425, Asp453, Arg463, Asp465, Arg534, Arg536, Tyr552, His553, Lys699, Tyr700, the Gly427-Leu428 chain (capped by CHO moiety of the Phe426 at the N-terminus and  $\text{NH}-\text{CH}_3$  moiety of the Leu429 residue at the C-terminus), the Ser517-Asp520 chain (capped by CHO moiety of the Gly516 at the N-terminus and  $\text{NH}-\text{CH}_3$  moiety of the Phe521), and six to eight water molecules in the vicinity of the active site. It resulted in fairly large QM system of  $\sim 350$  atoms.

**Quantum Chemical Calculations.** All quantum chemical calculations were performed at the density functional theory (DFT) level. Geometry optimizations were carried out at the Perdew–Burke–Ernzerhof (PBE) level.<sup>49</sup> The DFT/PBE calculations were expedited by expanding the Coulomb integrals in an auxiliary basis set, the resolution-of-identity (RI-J) approximation.<sup>50</sup> In QM/MM optimizations, the def2-SVP basis set was employed for all atoms.<sup>51</sup> The calculations of the interaction energy of the nonpolar side chains of the inhibitors with the S1' residues and its decomposition into the pair

contributions were carried out using the recent DFT-D3 computational protocol (DFT with the empirical dispersion) of Grimme<sup>52</sup> that was shown to yield, in combination with the B-LYP functional<sup>53</sup> and TZVPP basis set,<sup>51</sup> excellent values of the interaction energies for noncovalently bound complexes.

## ■ ASSOCIATED CONTENT

**S** **Supporting Information.** Details of data collection and refinement statistics, spectroscopic data for inhibitors, and QM/MM calculations together with resulting PDB structures. This material is available free of charge via the Internet at <http://pubs.acs.org>.

## Accession Codes

<sup>†</sup>Atomic coordinates of the present structures together with the experimental structure factor amplitudes were deposited at the RCSB Protein Data Bank under accession numbers 3SJX [GCPII-(E424A)/NAAM], 3SJJ [GCPII(E424A)/7S], 3SJE [GCPII-(E424A)/8S], and 3SJF (GCPII/9I).

## ■ AUTHOR INFORMATION

### Corresponding Author

\*Phone: +420-296-443-615. Fax: +420-296-443-610. E-mail: [cyril.barinka@img.cas.cz](mailto:cyril.barinka@img.cas.cz).

### Author Contributions

• These authors contributed equally.

## ■ ACKNOWLEDGMENT

The authors thank Jana Starkova for excellent technical assistance. Financial support from EMBO (Installation Grant No. 1978), Ministry of Education, Youth and Sports of the Czech Republic (Projects ME10031, LC 512), IBT (Grant AV0Z-50520701), and IOCB (Grant AV0Z40550506) is gratefully acknowledged. This work was also supported in part by the Intramural Research Program of the NIH, National Cancer Institute, Center for Cancer Research (J.L. and C.B.) and by Grant R21/R33 MH080580 (M.P.). Use of the Advanced Photon Source was supported by the U.S. Department of Energy, Office of Science, Office of Basic Energy Sciences, under Contract No. W-31-109-Eng38.

## ■ ABBREVIATIONS USED

rhGCPII, recombinant human glutamate carboxypeptidase II; QM/MM, quantum mechanics/molecular mechanics; NAAM, *N*-acetyl-aspartyl-methionine; NAAG, *N*-acetyl-aspartyl-glutamate; ANO, 2-aminononanoic acid; AOC, 2-aminooctanoic acid; SAR, structure–activity relationship; ESI-MS, electrospray ionization mass spectrometry; PET, positron emission tomography; Ac, acetyl group; GCPII, glutamate carboxypeptidase II; SPECT-CT, single photon emission computed tomography; HPLC, high performance liquid chromatography; DFT, density functional theory; PBE, Perdew–Burke–Ernzerhof; PCa, prostate cancer

## ■ REFERENCES

(1) Robinson, M. B.; Blakely, R. D.; Couto, R.; Coyle, J. T. Hydrolysis of the brain dipeptide *N*-acetyl-L-aspartyl-L-glutamate. Identification and characterization of a novel *N*-acetylated alpha-linked acidic dipeptidase activity from rat brain. *J. Biol. Chem.* **1987**, *262*, 14498–14506.

(2) Sacha, P.; Zamecnik, J.; Barinka, C.; Hlouchova, K.; Vicha, A.; Mlcochova, P.; Hilgert, I.; Eckschlager, T.; Konvalinka, J. Expression of glutamate carboxypeptidase II in human brain. *Neuroscience* **2007**, *144*, 1361–1372.

(3) Sokoloff, R. L.; Norton, K. C.; Gasior, C. L.; Marker, K. M.; Grauer, L. S. A dual-monoclonal sandwich assay for prostate-specific membrane antigen: levels in tissues, seminal fluid and urine. *Prostate* **2000**, *43*, 150–157.

(4) Banerjee, S. R.; Pullambhatla, M.; Byun, Y.; Nimmagadda, S.; Green, G.; Fox, J. J.; Horti, A.; Mease, R. C.; Pomper, M. G. <sup>68</sup>Ga-labeled inhibitors of prostate-specific membrane antigen (PSMA) for imaging prostate cancer. *J. Med. Chem.* **2010**, *53*, 5333–5341.

(5) Chen, Y.; Dhara, S.; Banerjee, S. R.; Byun, Y.; Pullambhatla, M.; Mease, R. C.; Pomper, M. G. A low molecular weight PSMA-based fluorescent imaging agent for cancer. *Biochem. Biophys. Res. Commun.* **2009**, *390*, 624–629.

(6) Rosenthal, S. A.; Haseman, M. K.; Polascik, T. J. Utility of capromab pendetide (ProstaScint) imaging in the management of prostate cancer. *Tech. Urol.* **2001**, *7*, 27–37.

(7) Zhang, A. X.; Murelli, R. P.; Barinka, C.; Michel, J.; Cocleaza, A.; Jorgensen, W. L.; Lubkowski, J.; Spiegel, D. A. A remote arene-binding site on prostate specific membrane antigen revealed by antibody-recruiting small molecules. *J. Am. Chem. Soc.* **2010**, *132*, 12711–12716.

(8) Zhou, J.; Neale, J. H.; Pomper, M. G.; Kozikowski, A. P. NAAG peptidase inhibitors and their potential for diagnosis and therapy. *Nat. Rev. Drug Discovery* **2005**, *4*, 1015–1026.

(9) Neale, J. H.; Olszewski, R. T.; Gehl, L. M.; Wroblewska, B.; Bzdega, T. The neurotransmitter *N*-acetylaspartylglutamate in models of pain, ALS, diabetic neuropathy, CNS injury and schizophrenia. *Trends Pharmacol. Sci.* **2005**, *26*, 477–484.

(10) Slusher, B. S.; Vornov, J. J.; Thomas, A. G.; Hurn, P. D.; Harukuni, I.; Bhardwaj, A.; Traystman, R. J.; Robinson, M. B.; Britton, P.; Lu, X. C.; Tortella, F. C.; Wozniak, K. M.; Yudkoff, M.; Potter, B. M.; Jackson, P. F. Selective inhibition of NAALADase, which converts NAAG to glutamate, reduces ischemic brain injury. *Nat. Med.* **1999**, *5*, 1396–1402.

(11) Zhang, W.; Slusher, B.; Murakawa, Y.; Wozniak, K. M.; Tsukamoto, T.; Jackson, P. F.; Sima, A. A. GCPII (NAALADase) inhibition prevents long-term diabetic neuropathy in type 1 diabetic BB/Wor rats. *J. Neurol. Sci.* **2002**, *194*, 21–28.

(12) Ghadge, G. D.; Slusher, B. S.; Bodner, A.; Canto, M. D.; Wozniak, K.; Thomas, A. G.; Rojas, C.; Tsukamoto, T.; Majer, P.; Miller, R. J.; Monti, A. L.; Roos, R. P. Glutamate carboxypeptidase II inhibition protects motor neurons from death in familial amyotrophic lateral sclerosis models. *Proc. Natl. Acad. Sci. U.S.A.* **2003**, *100*, 9554–9559.

(13) Carpenter, K. J.; Sen, S.; Matthews, E. A.; Flatters, S. L.; Wozniak, K. M.; Slusher, B. S.; Dickenson, A. H. Effects of GCP-II inhibition on responses of dorsal horn neurones after inflammation and neuropathy: an electrophysiological study in the rat. *Neuropeptides* **2003**, *37*, 298–306.

(14) Chen, S. R.; Wozniak, K. M.; Slusher, B. S.; Pan, H. L. Effect of 2-(phosphono-methyl)-pentanedioic acid on allodynia and afferent ectopic discharges in a rat model of neuropathic pain. *J. Pharmacol. Exp. Ther.* **2002**, *300*, 662–667.

(15) Yamamoto, T.; Nozaki-Taguchi, N.; Sakashita, Y.; Inagaki, T. Inhibition of spinal *N*-acetylated-alpha-linked acidic dipeptidase produces an antinociceptive effect in the rat formalin test. *Neuroscience* **2001**, *102*, 473–479.

(16) Olszewski, R. T.; Bukhari, N.; Zhou, J.; Kozikowski, A. P.; Wroblewski, J. T.; Shamimi-Noori, S.; Wroblewska, B.; Bzdega, T.; Vicini, S.; Barton, F. B.; Neale, J. H. NAAG peptidase inhibition reduces locomotor activity and some stereotypes in the PCP model of schizophrenia via group II mGluR. *J. Neurochem.* **2004**, *89*, 876–885.

(17) Kozela, E.; Wrobel, M.; Kos, T.; Wojcikowski, J.; Daniel, W. A.; Wozniak, K. M.; Slusher, B. S.; Popik, P. 2-MPPA, a selective glutamate carboxypeptidase II inhibitor, attenuates morphine tolerance but not dependence in C57/Bl mice. *Psychopharmacology (Berlin, Ger.)* **2005**, *183*, 275–284.

- (18) Popik, P.; Kozela, E.; Wrobel, M.; Wozniak, K. M.; Slusher, B. S. Morphine tolerance and reward but not expression of morphine dependence are inhibited by the selective glutamate carboxypeptidase II (GCP II, NAALADase) inhibitor, 2-PMPA. *Neuropsychopharmacology* **2003**, *28*, 457–467.
- (19) Guilarte, T. R.; Hammoud, D. A.; McGlothlan, J. L.; Caffo, B. S.; Foss, C. A.; Kozikowski, A. P.; Pomper, M. G. Dysregulation of glutamate carboxypeptidase II in psychiatric disease. *Schizophr. Res.* **2008**, *99*, 324–332.
- (20) Guilarte, T. R.; McGlothlan, J. L.; Foss, C. A.; Zhou, J.; Heston, W. D.; Kozikowski, A. P.; Pomper, M. G. Glutamate carboxypeptidase II levels in rodent brain using [<sup>125</sup>I]DCIT quantitative autoradiography. *Neurosci. Lett.* **2005**, *387*, 141–144.
- (21) Barinka, C.; Rinnova, M.; Sacha, P.; Rojas, C.; Majer, P.; Slusher, B. S.; Konvalinka, J. Substrate specificity, inhibition and enzymological analysis of recombinant human glutamate carboxypeptidase II. *J. Neurochem.* **2002**, *80*, 477–487.
- (22) Mlcochova, P.; Plechanovova, A.; Barinka, C.; Mahadevan, D.; Saldanha, J. W.; Rulisek, L.; Konvalinka, J. Mapping of the active site of glutamate carboxypeptidase II by site-directed mutagenesis. *FEBS J.* **2007**, *274*, 4731–4741.
- (23) Klusak, V.; Barinka, C.; Plechanovova, A.; Mlcochova, P.; Konvalinka, J.; Rulisek, L.; Lubkowski, J. Reaction mechanism of glutamate carboxypeptidase II revealed by mutagenesis, X-ray crystallography, and computational methods. *Biochemistry* **2009**, *48*, 4126–4138.
- (24) Barinka, C.; Byun, Y.; Dusich, C. L.; Banerjee, S. R.; Chen, Y.; Castanares, M.; Kozikowski, A. P.; Mease, R. C.; Pomper, M. G.; Lubkowski, J. Interactions between human glutamate carboxypeptidase II and urea-based inhibitors: structural characterization. *J. Med. Chem.* **2008**, *51*, 7737–7743.
- (25) Barinka, C.; Hlouchova, K.; Rovenska, M.; Majer, P.; Dauter, M.; Hin, N.; Ko, Y. S.; Tsukamoto, T.; Slusher, B. S.; Konvalinka, J.; Lubkowski, J. Structural basis of interactions between human glutamate carboxypeptidase II and its substrate analogs. *J. Mol. Biol.* **2008**, *376*, 1438–1450.
- (26) Jackson, P. F.; Tays, K. L.; Maclin, K. M.; Ko, Y. S.; Li, W.; Vitharana, D.; Tsukamoto, T.; Stoermer, D.; Lu, X. C.; Wozniak, K.; Slusher, B. S. Design and pharmacological activity of phosphinic acid based NAALADase inhibitors. *J. Med. Chem.* **2001**, *44*, 4170–4175.
- (27) Kozikowski, A. P.; Nan, F.; Conti, P.; Zhang, J.; Ramadan, E.; Bzdega, T.; Wroblewska, B.; Neale, J. H.; Pshenichkin, S.; Wroblewski, J. T. Design of remarkably simple, yet potent urea-based inhibitors of glutamate carboxypeptidase II (NAALADase). *J. Med. Chem.* **2001**, *44*, 298–301.
- (28) Liu, T.; Toriyabe, Y.; Kazak, M.; Berkman, C. E. Pseudoirreversible inhibition of prostate-specific membrane antigen by phosphoramidate peptidomimetics. *Biochemistry* **2008**, *47*, 12658–12660.
- (29) Hlouchova, K.; Barinka, C.; Klusak, V.; Sacha, P.; Mlcochova, P.; Majer, P.; Rulisek, L.; Konvalinka, J. Biochemical characterization of human glutamate carboxypeptidase III. *J. Neurochem.* **2007**, *101*, 682–696.
- (30) Vitharana, D.; France, J. E.; Scarpetti, D.; Bonneville, G. W.; Majer, P.; Tsukamoto, T. Synthesis and biological evaluation of (R)- and (S)-2-(phosphonomethyl)pentanedioic acids as inhibitors of glutamate carboxypeptidase II. *Tetrahedron: Asymmetry* **2002**, *13*, 1609–1614.
- (31) Barinka, C.; Rovenska, M.; Mlcochova, P.; Hlouchova, K.; Plechanovova, A.; Majer, P.; Tsukamoto, T.; Slusher, B. S.; Konvalinka, J.; Lubkowski, J. Structural insight into the pharmacophore pocket of human glutamate carboxypeptidase II. *J. Med. Chem.* **2007**, *50*, 3267–3273.
- (32) Wang, H.; Byun, Y.; Barinka, C.; Pullambhatla, M.; Bhang, H. E.; Fox, J. J.; Lubkowski, J.; Mease, R. C.; Pomper, M. G. Bioisosterism of urea-based GCPII inhibitors: synthesis and structure–activity relationship studies. *Bioorg. Med. Chem. Lett.* **2010**, *20*, 392–397.
- (33) Majer, P.; Hin, B.; Stoermer, D.; Adams, J.; Xu, W.; Duvall, B. R.; Delahanty, G.; Liu, Q.; Stathis, M. J.; Wozniak, K. M.; Slusher, B. S.; Tsukamoto, T. Structural optimization of thiol-based inhibitors of glutamate carboxypeptidase II by modification of the P1' side chain. *J. Med. Chem.* **2006**, *49*, 2876–2885.
- (34) Kozikowski, A. P.; Zhang, J.; Nan, F.; Petukhov, P. A.; Grajkowska, E.; Wroblewski, J. T.; Yamamoto, T.; Bzdega, T.; Wroblewska, B.; Neale, J. H. Synthesis of urea-based inhibitors as active site probes of glutamate carboxypeptidase II: efficacy as analgesic agents. *J. Med. Chem.* **2004**, *47*, 1729–1738.
- (35) Mease, R. C.; Dusich, C. L.; Foss, C. A.; Ravert, H. T.; Dannels, R. F.; Seidel, J.; Prideaux, A.; Fox, J. J.; Sgouros, G.; Kozikowski, A. P.; Pomper, M. G. N-[N-[(S)-1,3-Dicarboxypropyl]carbonyl]-4-[<sup>18</sup>F]fluorobenzyl-L-cysteine, [<sup>18</sup>F]DCFBC: a new imaging probe for prostate cancer. *Clin. Cancer Res.* **2008**, *14*, 3036–3043.
- (36) Gingras, R.; Richard, C.; El-Alfy, M.; Morales, C. R.; Potier, M.; Pshezhetsky, A. V. Purification, cDNA cloning, and expression of a new human blood plasma glutamate carboxypeptidase homologous to N-acetyl-aspartyl-alpha-glutamate carboxypeptidase/prostate-specific membrane antigen. *J. Biol. Chem.* **1999**, *274*, 11742–11750.
- (37) Zajc, T.; Suban, D.; Rajkovic, J.; Dolenc, I. Baculoviral expression and characterization of human recombinant PGCP in the form of an active mature dimer and an inactive precursor protein. *Protein Expression Purif.* **2011**, *75*, 119–126.
- (38) Otwinowski, Z.; Minor, W. Processing of X-ray Diffraction Data Collected in Oscillation Mode. In *Methods in Enzymology*; Carter, C. W., Jr., Sweet, R. M., Eds.; Academic Press: New York, 1997; pp 307–326; Vol. 276.
- (39) Barinka, C.; Starkova, J.; Konvalinka, J.; Lubkowski, J. A high-resolution structure of ligand-free human glutamate carboxypeptidase II. *Acta Crystallogr., Sect. F: Struct. Biol. Cryst. Commun.* **2007**, *63*, 150–153.
- (40) Murshudov, G. N.; Vagin, A. A.; Lebedev, A.; Wilson, K. S.; Dodson, E. J. Efficient anisotropic refinement of macromolecular structures using FFT. *Acta Crystallogr., Sect. D: Biol. Crystallogr.* **1999**, *55*, 247–255.
- (41) Emsley, P.; Cowtan, K. Coot: model-building tools for molecular graphics. *Acta Crystallogr., Sect. D: Biol. Crystallogr.* **2004**, *60*, 2126–2132.
- (42) Schuttelkopf, A. W.; van Aalten, D. M. PRODRG: a tool for high-throughput crystallography of protein–ligand complexes. *Acta Crystallogr., Sect. D: Biol. Crystallogr.* **2004**, *60*, 1355–1363.
- (43) Davis, I. W.; Leaver-Fay, A.; Chen, V. B.; Block, J. N.; Kapral, G. J.; Wang, X.; Murray, L. W.; Arendall, W. B., III; Snoeyink, J.; Richardson, J. S.; Richardson, D. C. MolProbity: all-atom contacts and structure validation for proteins and nucleic acids. *Nucleic Acids Res.* **2007**, *35*, W375–W383.
- (44) Wang, S. S. p-Alkoxybenzyl alcohol resin and p-alkoxybenzylloxycarbonylhydrazide resin for solid phase synthesis of protected peptide fragments. *J. Am. Chem. Soc.* **1973**, *95*, 1328–1333.
- (45) Chen, Y.; Foss, C. A.; Byun, Y.; Nimmagadda, S.; Pullambhatla, M.; Fox, J. J.; Castanares, M.; Lupold, S. E.; Babich, J. W.; Mease, R. C.; Pomper, M. G. Radiohalogenated prostate-specific membrane antigen (PSMA)-based ureas as imaging agents for prostate cancer. *J. Med. Chem.* **2008**, *51*, 7933–7943.
- (46) Ryde, U. The coordination of the catalytic zinc ion in alcohol dehydrogenase studied by combined quantum-chemical and molecular mechanics calculations. *J. Comput.-Aided Mol. Des.* **1996**, *10*, 153–164.
- (47) Treutler, O.; Ahlrichs, R. Efficient molecular numerical-integration schemes. *J. Chem. Phys.* **1995**, *102*, 346–354.
- (48) Cornell, W. D.; Cieplak, P.; Bayly, C. I.; Gould, I. R.; Merz, K. M.; Ferguson, D. M.; Spellmeyer, D. C.; Fox, T.; Caldwell, J. W.; Kolman, P. A. A 2nd generation force-field for the simulation of proteins, nucleic-acids, and organic molecules. *J. Am. Chem. Soc.* **1995**, *117*, 5179–5197.
- (49) Perdew, J. P.; Burke, K.; Erzerhof, M. Generalized gradient approximation made simple. *Phys. Rev. Lett.* **1996**, *77*, 3865–3868.
- (50) Eichkorn, K.; Weigend, F.; Treutler, O.; Ahlrichs, R. Auxiliary basis sets for main row atoms and transition metals and their use to approximate Coulomb potentials. *Theor. Chim. Acta* **1997**, *97*, 119–124.
- (51) Weigend, F.; Ahlrichs, R. Balanced basis sets of split valence, triple zeta valence and quadruple zeta valence quality for H to Rn: design and assessment of accuracy. *Phys. Chem. Chem. Phys.* **2005**, *7*, 3297–3305.

(52) Grimme, S.; Antony, J.; Ehrlich, S.; Krieg, H. A consistent and accurate ab initio parametrization of density functional dispersion correction (DFT-D) for the 94 elements H–Pu. *J. Chem. Phys.* **2010**, *132*, 154104.

(53) Becke, A. D. Density-functional exchange-energy approximation with correct asymptotic behavior. *Phys. Rev. A* **1988**, *38*, 3098–3100.